

# **(Re)mind the gap: a hiatus in star formation history unveiled by APOGEE DR17**

E. Spitoni, F. Matteucci, R. Gratton, B. Ratcliffe, I. Minchev, and G. Cescutti

reporter: Zheng Yu

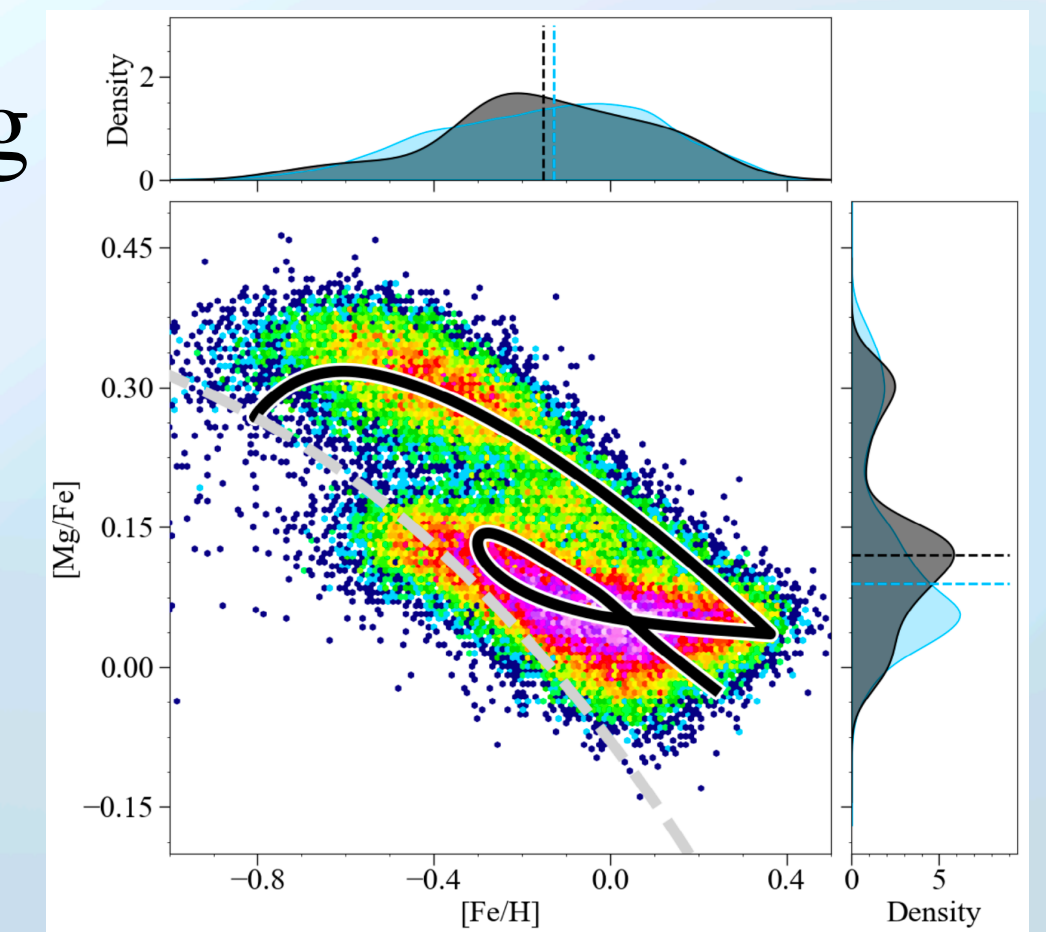
2024/06/07

# Introduction

**1. Research Background:** Understanding the chemical evolution of galaxies is key to uncovering their history. The Milky Way, with its rich data, is ideal for studying these processes. Stars in the Milky Way show a bimodal distribution in  $[\alpha/\text{Fe}]$  vs  $[\text{Fe}/\text{H}]$ , revealing high- $\alpha$  and low- $\alpha$  sequences tied to different star formation histories.

**2. Research Significance:** Understanding the hiatus between high- $\alpha$  and low- $\alpha$  sequences is crucial. This study explores the impact of dwarf galaxy accretion on the Milky Way. Using APOGEE DR17 data to refine models provides insights into our galaxy's evolution.

- Star Formation Hiatus: Clarifying this period helps define the Milky Way's timeline.
- Chemical Enrichment: Studying accreted dwarf galaxies enhances our understanding of the Milky Way's composition.
- Model Validation: Refining models with data ensures accuracy in representing galactic processes.





# Introduction

## The Two-Infall Model (E. Spitoni et al. 2019)

This model explains the Milky Way's chemical evolution through two gas accretion events.

- The 1st-infall formed the thick disc and high- $\alpha$  stars.

### Core-Collapse Supernovae (CC-SNe)



$\alpha$ - elements (e.g. O, Mg, Si)

- Hiatus - the star formation rates decrease significantly.

### Type Ia SNe      Time-delay

- The 2nd-infall later formed the thin disc and low- $\alpha$  stars.

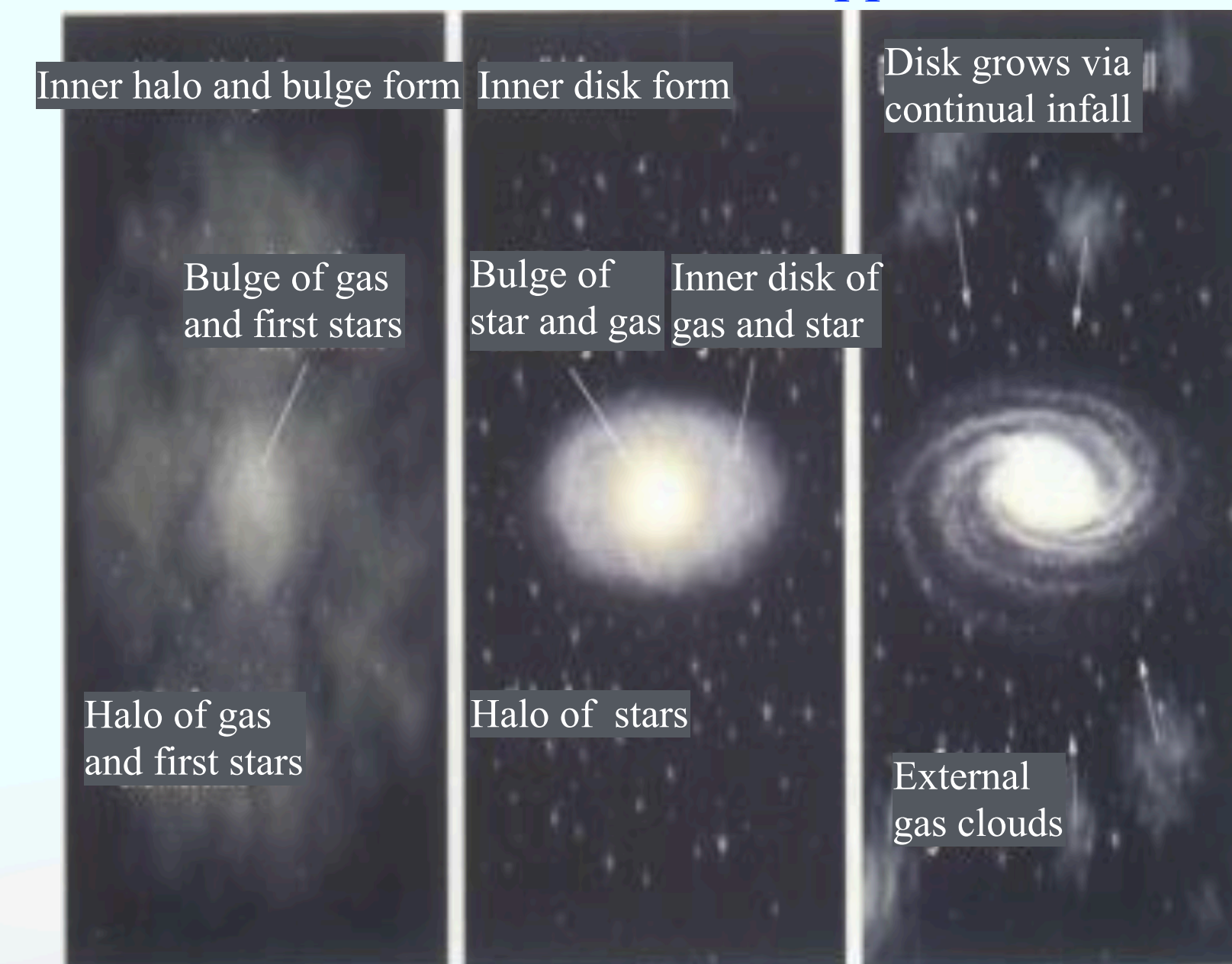
### Type Ia SNe



Fe

→ Clarifying the chemical bimodality.

C. Chiappini et al. 1997



During the first one the halo, bulge and part of thick disk formed, the second gave rise to the disk.



# Data

The APOGEE DR17 data sample

astroNN catalogue(Leung & Bovy 2019)

Signal-to-noise ratio ( $S/N$ )  $> 80$

A logarithm of surface gravity  $\log g < 3.5$

Galactocentric distances enclosed between 7 and 9 kpc

Vertical heights  $|z| < 2$  kpc

*Bimodality*

$$\Delta[\text{Fe}/\text{H}]_{\text{peak}} = [\text{Fe}/\text{H}]_{\text{peak,low}} - [\text{Fe}/\text{H}]_{\text{peak,high}} \simeq 0.42 \text{ dex.}$$
$$\gg \Delta[\alpha/\text{H}]_{\text{peak}}$$

spanned by  $\Delta[\alpha/\text{H}]_{\text{peak}}$ , revealing that  $\Delta[\text{Mg}/\text{H}]_{\text{peak}} = 0.18$  dex,  $\Delta[\text{Si}/\text{H}]_{\text{peak}} = 0.22$  dex, and  $\Delta[\text{O}/\text{H}]_{\text{peak}} = 0.13$  dex. The small-

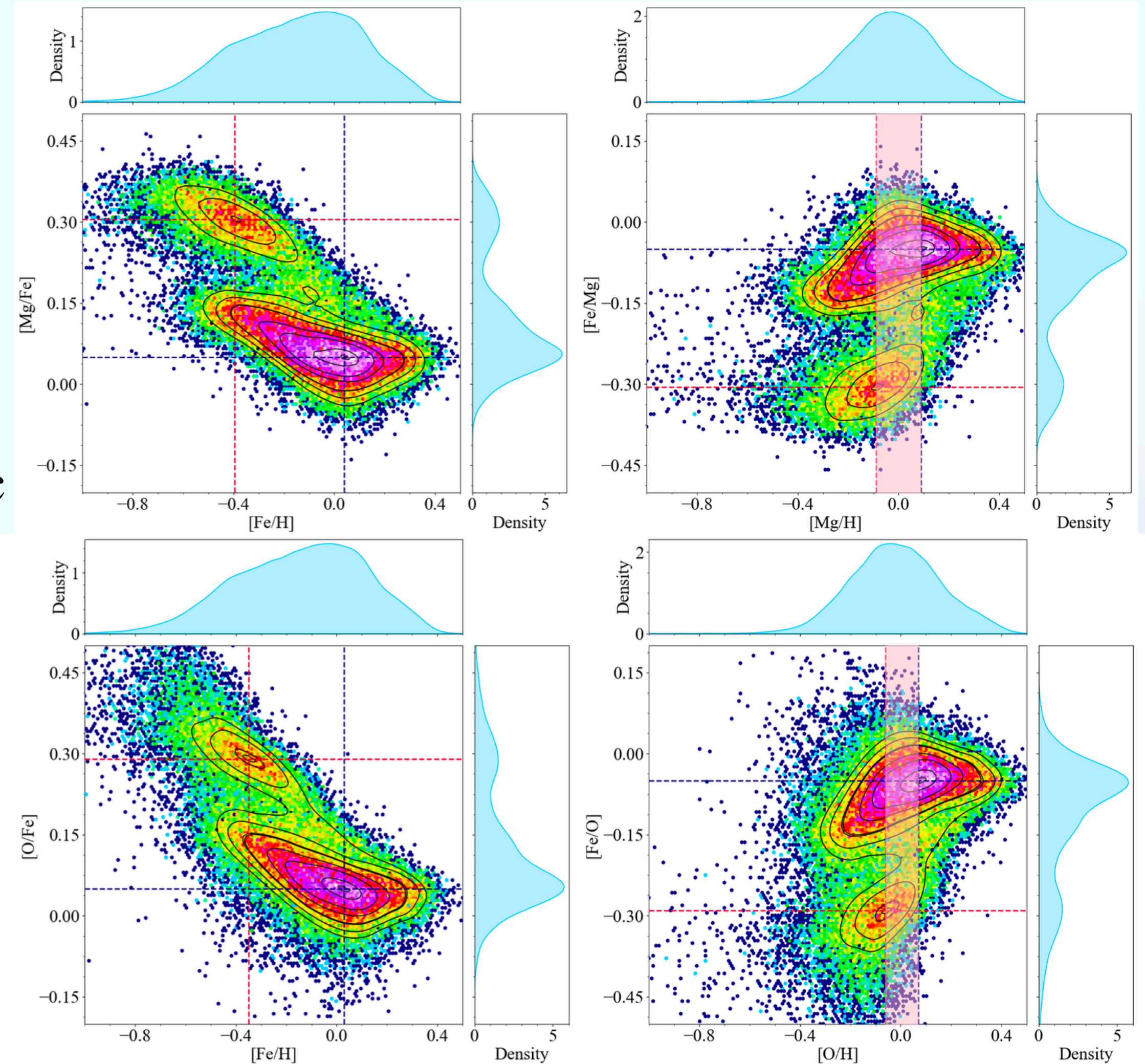


**Fig. 1.** Signatures of the hiatus in the star formation unveiled by APOGEE DR17 red giant stars. Density distribution of the observed  $[\alpha/\text{Fe}]$  versus  $[\text{Fe}/\text{H}]$  (left panels) and  $[\text{Fe}/\alpha]$  versus  $[\alpha/\text{H}]$  (right panels) abundance ratios from APOGEE DR17 (see text for data selection details) where  $\alpha=\text{Mg}$  (first row),  $\alpha=\text{Si}$  (second row), and  $\alpha=\text{O}$  (last row) are reported. On the sides of each panel, the normalised Kernel Density Estimation (KDE) calculated with a Gaussian kernel of the abundance ratio distributions are also reported. The coordinates of the densest regions for the high- $\alpha$  and low- $\alpha$  stars are pinpointed with red and blue lines, respectively. In the right panels, the shaded pink area spans the region of the quantity  $\Delta[\alpha/\text{H}]_{\text{peak}}$  as defined in eq. (1).



# Data

## The APOGEE DR17 data sample

### astroNN catalogue (Leung & Bovy 2019)

- Stars on the high- $\alpha$  sequence are likely to have migrated from the inner Galactic regions, indicated by small guiding radii and large eccentricities.
- The thick and thin discs are formed sequentially.

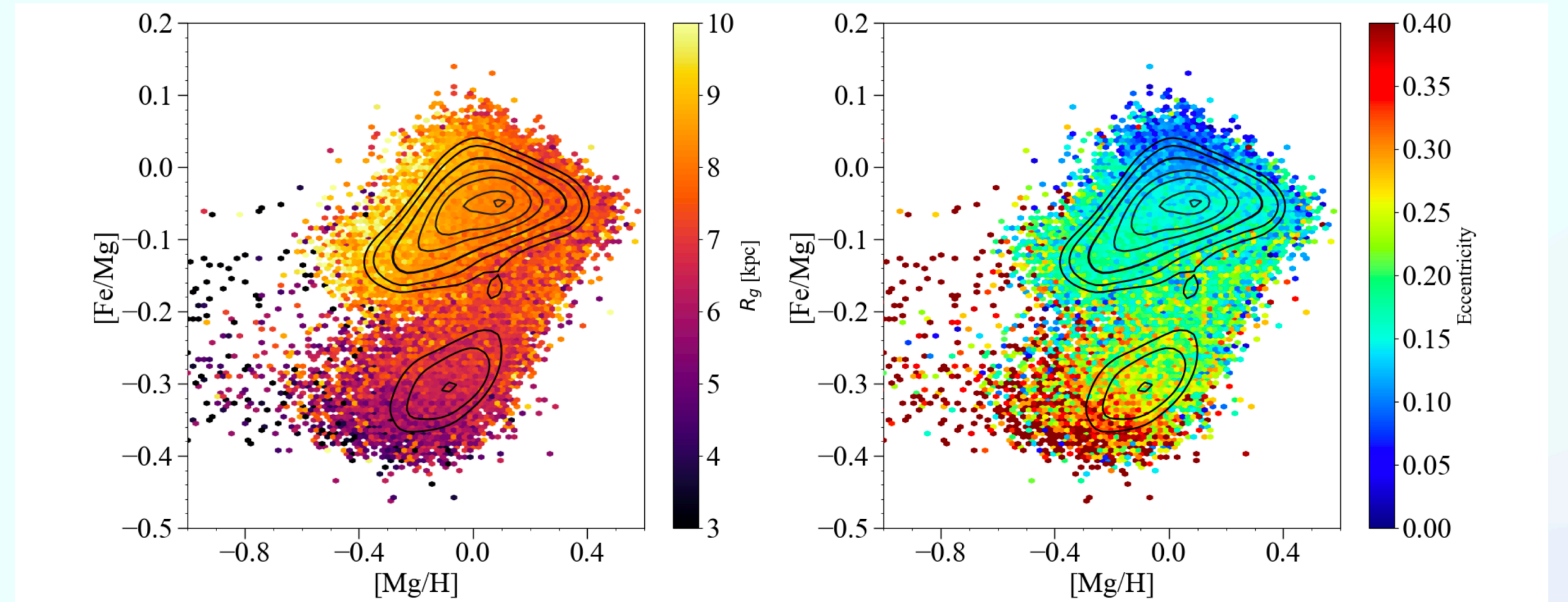


**Fig. 2.** Observed stellar  $[\text{Fe}/\text{Mg}]$  versus  $[\text{Mg}/\text{H}]$  abundance ratios from APOGEE DR17 as in the upper right panel of Fig. 1 colour coded with the median values of the guiding radii (left panel) and the eccentricity (right panel) as computed by the value added astroNN catalogue.

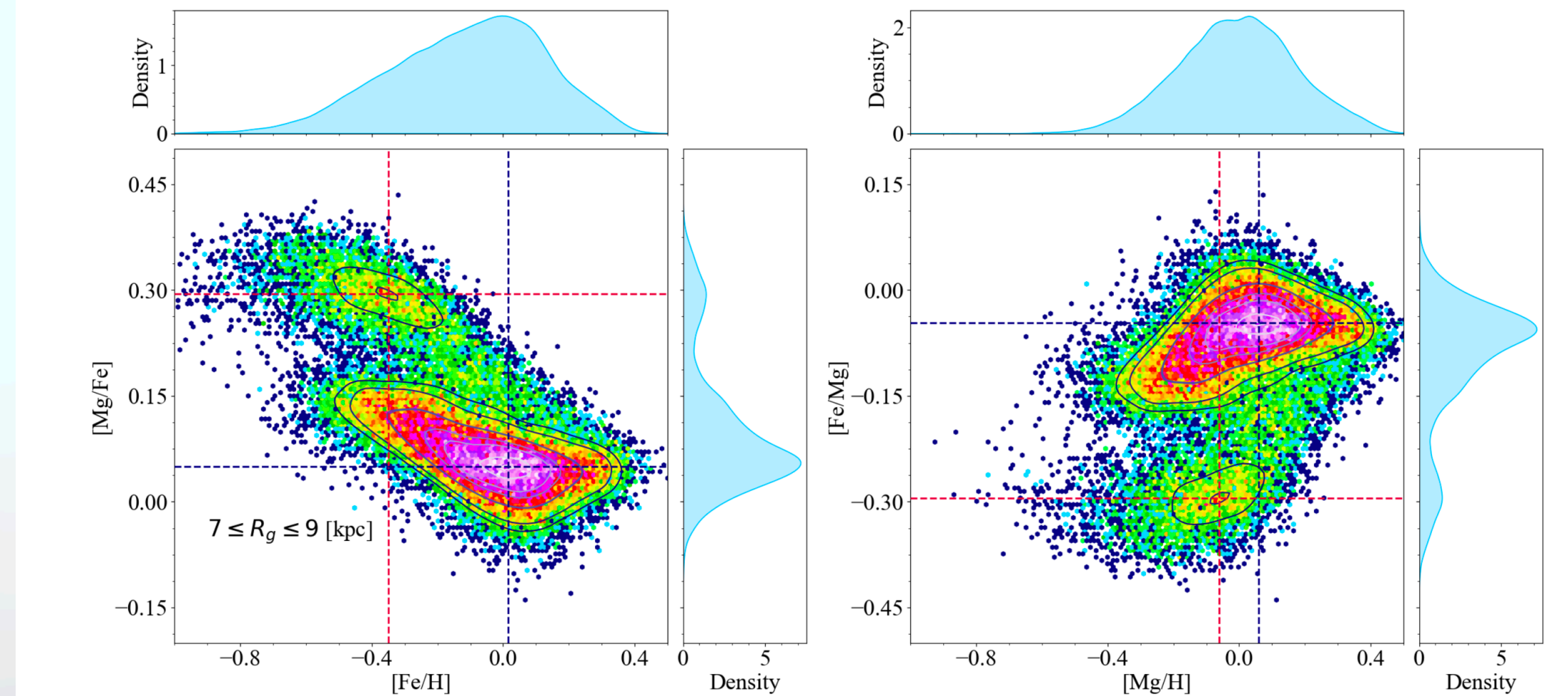


**Fig. 3.** As the upper panel of Fig. 1 but for APOGEE DR17 stars with guiding radii  $R_g$  between 7 and 9 kpc we do not impose condition on the Galactocentric distance as we did for Fig. 1) and vertical height  $|z| < 2$  kpc.



# Data

The APOGEE DR17 data sample

astroNN catalogue([Leung & Bovy 2019](#))

*The birth radii*

The gradient of metallicity, at birth, remains linear.

$$R_b(\text{age}, [\text{Fe}/\text{H}]) = \frac{[\text{Fe}/\text{H}](R_b, \tau) - [\text{Fe}/\text{H}](R = 0, \tau)}{\nabla[\text{Fe}/\text{H}]}$$

In the low- $\alpha$  sequence,

two clumps,

[Ratcliffe et al. \(2023\)](#) suggested that they could correlate with the triggered star formation due to the pericentric passages of Sagittarius galaxy.

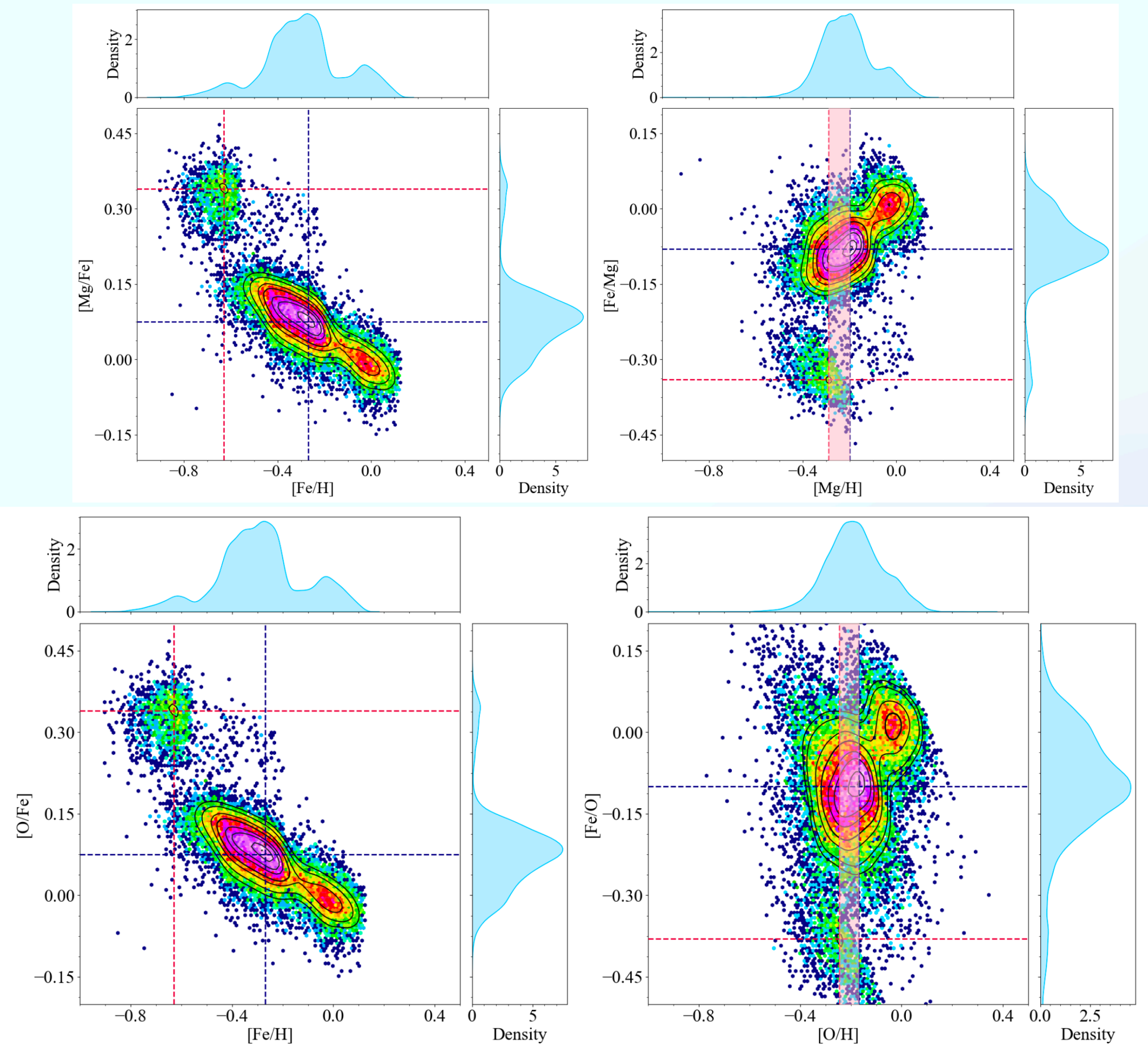


**Fig. 4.** As in Fig. 1 but for APOGEE DR17 stars with birth radii between 7 and 9 kpc. The birth radii were derived in [Ratcliffe et al. \(2023\)](#), following the methodology given in Section 2.2.



# Chemical evolution models

## The two-infall model for the MW disc components

The functional form of the adopted gas infall rate is:

1st infall, high- $\alpha$

2nd infall, low- $\alpha$

$$\mathcal{I}_i(t) = X_i \left( \overbrace{A e^{-t/T_{\text{high}}}}^{\text{1st infall, high-}\alpha} + \overbrace{\theta(t - T_{\text{max}}) B e^{-(t-T_{\text{max}})/T_{\text{low}}}}^{\text{2nd infall, low-}\alpha} \right)$$

$T_{\text{high}}, T_{\text{low}}$ : the timescales of the two distinct gas infall episodes.

$\theta$ : The Heaviside step function.

$X_i$ : the abundance by mass unit of the element  $i$ .

$A$  and  $B$ : obtained by imposing a fit to the observed current.

total surface mass density in the solar neighbourhood.

Initial stellar mass function (IMF)

Scalo (1986) constant in time and space.

Star formation rates:

$$\psi(t) \propto \nu_{\text{high,low}} \cdot \sigma_g(t)^k$$

**Table 1.** Summary of the main parameters of the two-infall model presented in this study (see Section 3.1): the accretion timescales ( $T_{\text{high}}, T_{\text{low}}$ ), time-delay  $T_{\text{max}}$ , and the star formation efficiencies ( $\nu_{\text{low}}, \nu_{\text{high}}$ , the present-day total surface mass density ratios  $\sigma_{\text{low}}/\sigma_{\text{high}}$ ). Finally, the infall chemical composition is indicated in the last column. We also specify the values corresponding to those adopted in the revised version of the Spitoni et al. (2019b) two-infall chemical evolution model presented in Nissen et al. (2020).

Model MW	$T_{\text{high}}$ [Gyr]	$T_{\text{low}}$ [Gyr]	$T_{\text{max}}$ [Gyr]	$\nu_{\text{high}}$ [Gyr <sup>-1</sup> ]	$\nu_{\text{low}}$ [Gyr <sup>-1</sup> ]	$\sigma_{\text{low}}/\sigma_{\text{high}}$	$X_i$
	0.377	3.203	3.519	2.000	1.000	2.500	Enriched (Section 3.2)
	Nissen et al. (2020)						

# Chemical evolution models

## The chemical evolution model for a massive dwarf galaxy

- A "typical" dwarf galaxy that can be accreted after an evolutionary time of 1.3 Gyr (12.5 Gyr ago).
- An infall time-scale of 0.24 Gyr.
- The SFE = 0.42 Gyr<sup>-1</sup> (Vincenzo et al. 2019)

A galactic wind proportional to the SFR:

Kennicutt (1998)

$$W(t) = \omega \psi(t)$$

**Table 1.** Summary of the main parameters of the two-infall model presented in this study (see Section 3.1): the accretion timescales ( $T_{\text{high}}$ ,  $T_{\text{low}}$ ), time-delay  $T_{\text{max}}$ , and the star formation efficiencies ( $\nu_{\text{low}}$ ,  $\nu_{\text{high}}$ , the present-day total surface mass density ratios  $\sigma_{\text{low}}/\sigma_{\text{high}}$ ). Finally, the infall chemical composition is indicated in the last column. We also specify the values corresponding to those adopted in the revised version of the Spitoni et al. (2019b) two-infall chemical evolution model presented in Nissen et al. (2020).

Model MW	$T_{\text{high}}$ [Gyr]	$T_{\text{low}}$ [Gyr]	$T_{\text{max}}$ [Gyr]	$\nu_{\text{high}}$ [Gyr <sup>-1</sup> ]	$\nu_{\text{low}}$ [Gyr <sup>-1</sup> ]	$\sigma_{\text{low}}/\sigma_{\text{high}}$	$X_i$
	0.377	3.203	3.519	2.000	1.000	2.500	Enriched (Section 3.2)
	Nissen et al. (2020)						

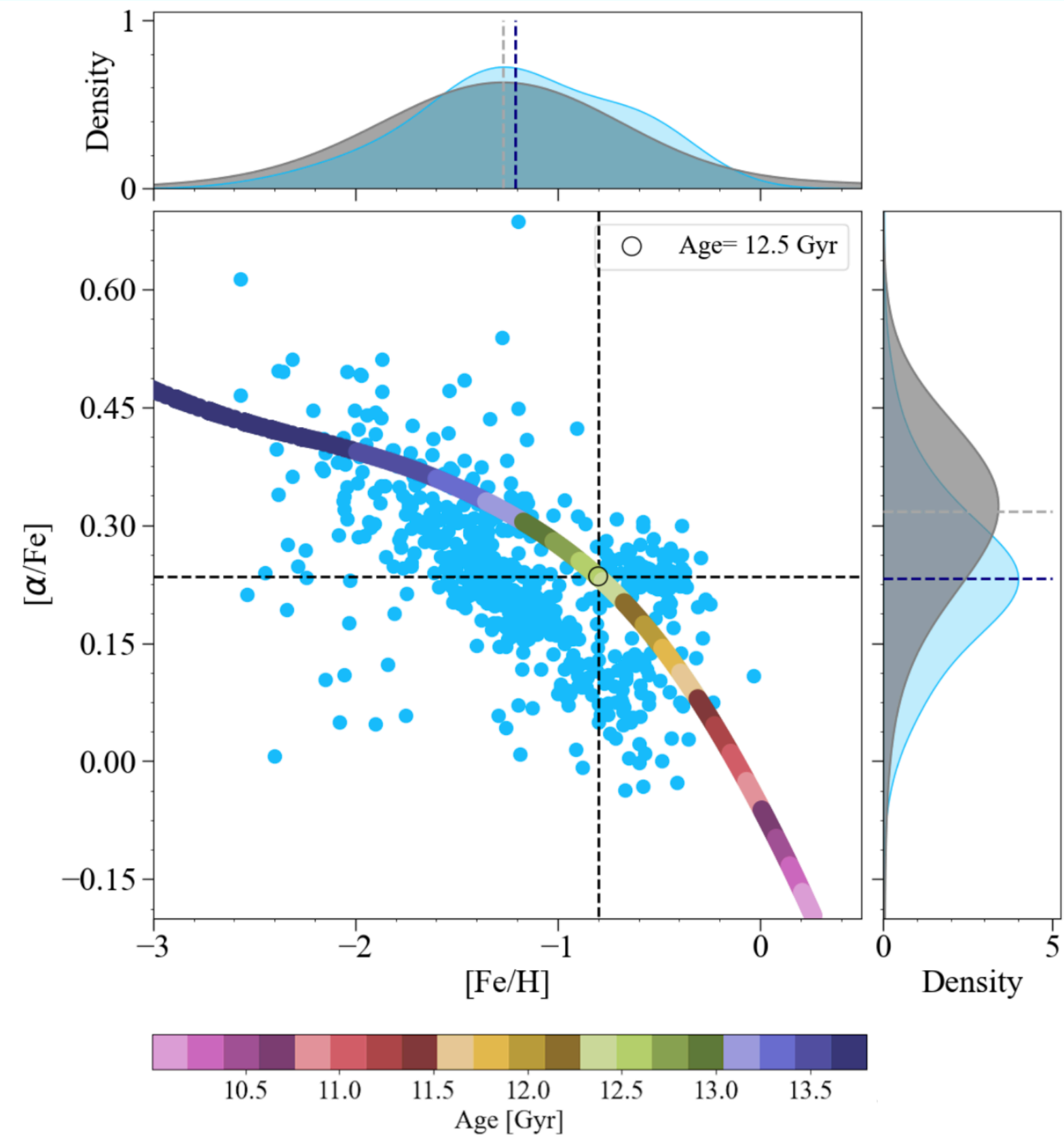


**Fig. 5.**  $[\alpha/\text{Fe}]$  versus  $[\text{Fe}/\text{H}]$  predicted by the accreted dwarf satellite presented in Section 3.2. The coloured coding stands for the galactic ages at different evolutionary phases. With the empty circle, the chemical abundance ratio at an age of 12.5 Gyr is reported. With light-blue points, we labelled Enceladus stars as suggested by Helmi et al. (2018). On the sides of each panel the observed (light-blue shaded area) and predicted (dark-grey shaded area) normalised KDE of the abundance ratio distributions calculated with a Gaussian kernel are also reported.



# Results

## Comparison with APOGEE DR17 data

- The late accretion of pristine gas produced a dilution of the chemical abundances of the metals thus producing an almost constant  $[\alpha/\text{Fe}]$  ratio and a decreasing  $[\text{Fe}/\text{H}]$ .
- The CC-SNe induce a sharp increase of the  $[\alpha/\text{Fe}]$  ratio.
- Type Ia SNe: a decrease and a shift towards higher metallicities.

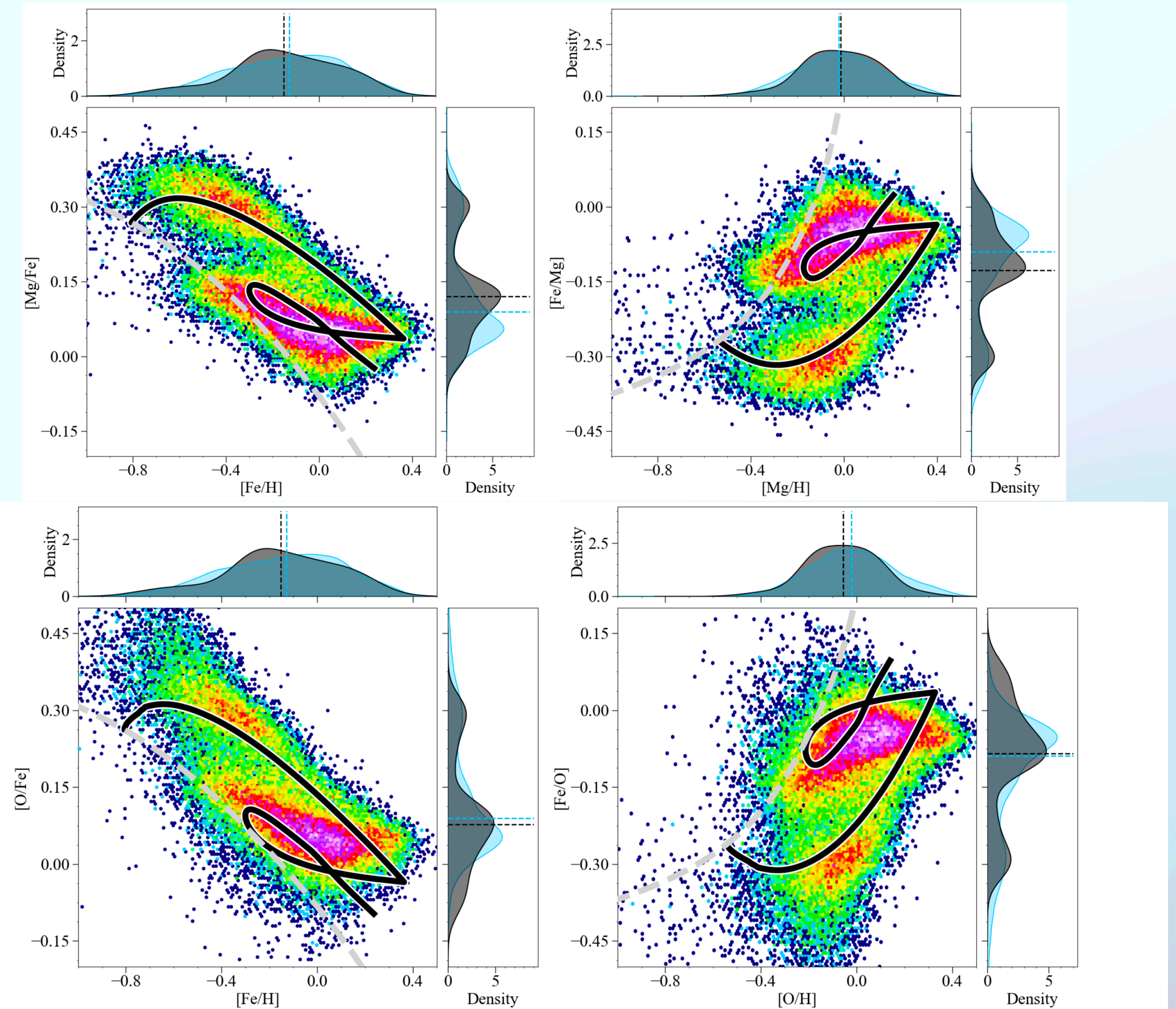


**Fig. 6.** Comparison between predicted (black solid lines, see Section 3.1 for the two-infall model description) and observed APOGEE DR17

# Results

## Signatures of the SF hiatus in the predicted abundance ratios

$$\Delta[\text{Fe}/\text{H}]_{\text{median}} = [\text{Fe}/\text{H}]_{\text{median low}} - [\text{Fe}/\text{H}]_{\text{median high}} \simeq 0.23 \text{ dex}$$

ining the right panels of Fig. 7 for the studied  $\alpha$ -elements, we observe the following median variations:  $\Delta[\text{Mg}/\text{H}]_{\text{median}} = 0.05$  dex,  $\Delta[\text{Si}/\text{H}]_{\text{median}} = 0.09$  dex, and  $\Delta[\text{O}/\text{H}]_{\text{median}} = 0.03$  dex. Hence, we have that  $\Delta[\alpha/\text{H}]_{\text{median}} \ll \Delta[\text{Fe}/\text{H}]_{\text{median}}$ . Moreover, the

These trends are in agreement with the findings from APOGEE DR17 data.

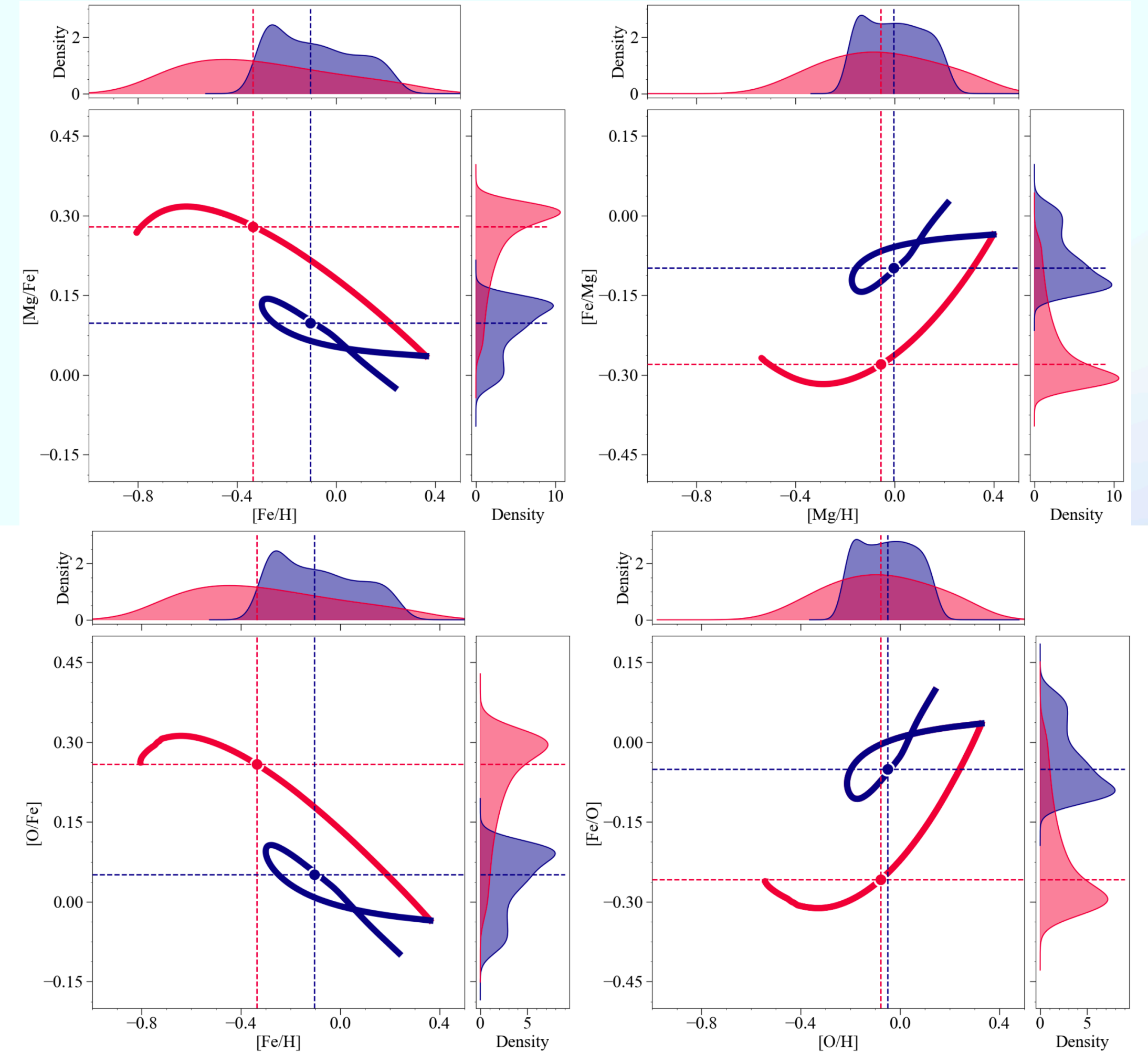


**Fig. 7.** Stellar distributions in the  $[\alpha/\text{Fe}]$  versus  $[\text{Fe}/\text{H}]$  (left panels) and  $[\text{Fe}/\alpha]$  versus  $[\alpha/\text{H}]$  (right panels) spaces for  $\alpha=\text{Mg}$  (upper panels),  $\alpha=\text{Si}$  (middle panels) and  $\alpha=\text{O}$  (lower panels) predicted by the two-infall model for the high- $\alpha$  phases (red lines) and distributions, spanning evolutionary time  $t < T_{\text{max}}$  and for the low- $\alpha$  ones (blue lines) and distributions, for  $t \geq T_{\text{max}}$ . The associated median values of the distributions are reported with dashed coloured lines and the associated points in the abundance ratio spaces with coloured points. Each distribution is normalised in order that its area is 1.



# Results

## Counting of the stars throughout the high- and low- $\alpha$ sequences

The chemical evolution model reproduces remarkably well this chemical dissection of the disc.

The "almost" horizontal phase  
— a negligible number of stars.

The effect of dilution by gas infall  
strongly depressed star formation.

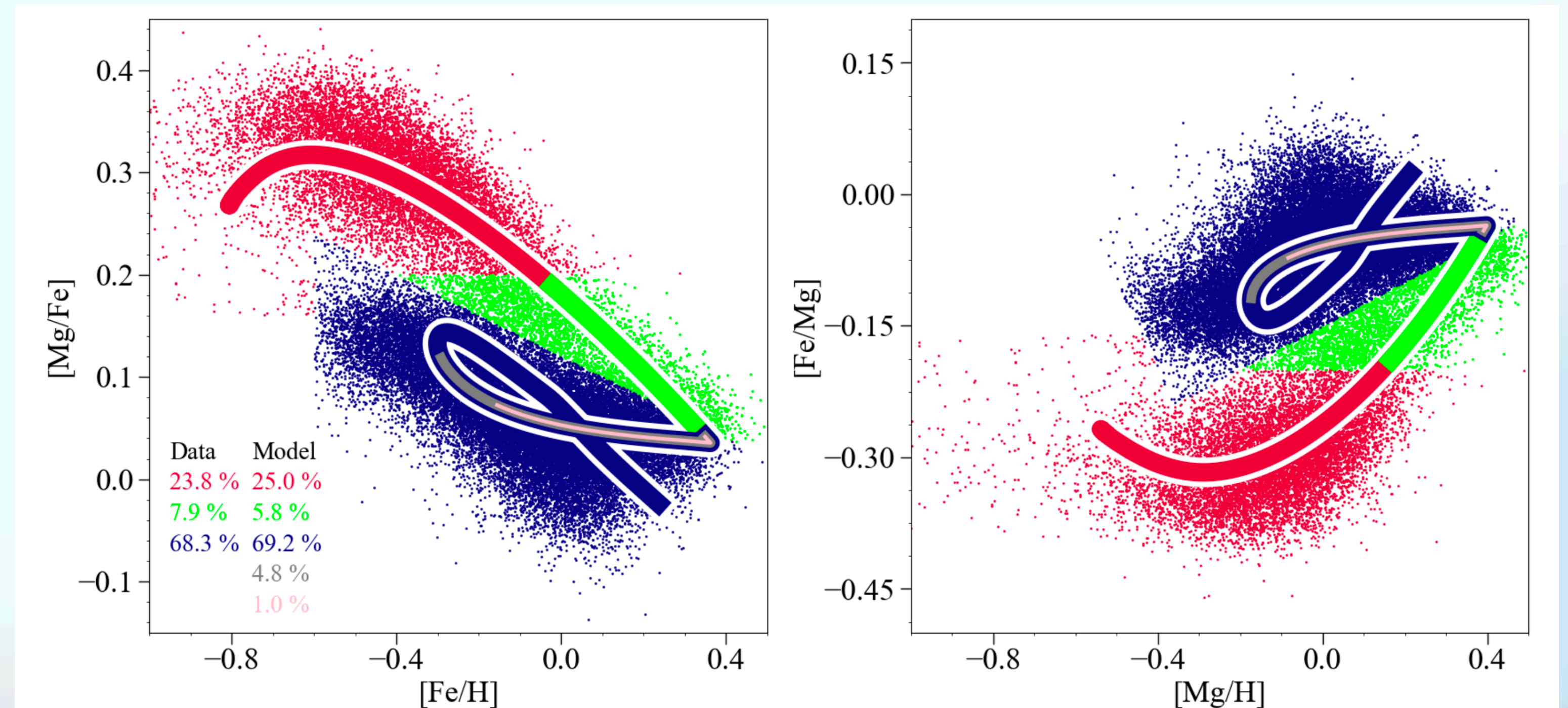


**Fig. 8.** Counting of the stars throughout the high- $\alpha$  and low- $\alpha$  sequences. Comparison between predicted and observed distributions of stars in 3 regions of the  $[Mg/Fe]$  versus  $[Fe/H]$  (left panel) and  $[Fe/Mg]$  versus  $[Mg/H]$  (right panel) abundance ratios highlighted in red, green and blue. The respective percentages of stars are reported in the legend in the leftmost plot. For the model prediction, we also indicate the percentage of stars which lie in the dilution phase of the low- $\alpha$  in the chemical evolution tracks highlighted with grey and pink lines.

# Conclusions

## **Effectiveness of the Two-Infall Model:**

- The two-infall model effectively explains the chemical composition and evolution of thick and thin disc stars in the Milky Way.
- The two gas-infall events and subsequent star formation activities are crucial to the galaxy's chemical evolution.

## **Variation in $\alpha$ -Elements and Metal Abundances:**

- Core-collapse supernovae (CC-SNe) rapidly increase the abundance of  $\alpha$ -elements in the early stages, leading to a temporary rise in the  $[\alpha/\text{Fe}]$  ratio.
- Type Ia supernovae increase the metal abundance, balancing the  $[\alpha/\text{Fe}]$  ratio.

## **Impact of the Hiatus Period:**

- The hiatus period between the two infall events results in a significant decrease in the star formation rate.
- The hiatus explains the bimodality of  $\alpha$ -elements.

## **Influence of External Galaxies:**

- The pericentric passages of the Sagittarius dwarf galaxy significantly impact the star formation history of the Milky Way, especially within the low- $\alpha$  sequence stellar populations.